HHS Public Access

Author manuscript

Nat Med. Author manuscript; available in PMC 2011 March 01.

Published in final edited form as:

Nat Med. 2010 September ; 16(9): 1035–1041. doi:10.1038/nm.2198.

Therapeutic cell engineering using surface-conjugated synthetic nanoparticles

Matthias T. Stephan[1,2], **James J. Moon**[1,2], **Soong Ho Um**[1,2,3], **Anna Bershteyn**[1,2], and **Darrell J. Irvine**[1,2,3,4,5,‡]

[1]Department of Material Science and Engineering, Massachusetts Institute of Technology, Cambridge, MA 02139, USA

[2]Koch Institute for Integrative Cancer Research, Massachusetts Institute of Technology, Cambridge, MA 02139, USA

[3]Department of Biological Engineering, Massachusetts Institute of Technology, Cambridge, MA 02139, USA

[4] Ragon Institute of MGH, MIT, and Harvard, Boston, MA 02139, USA

[5] Howard Hughes Medical Institute, 4000 Jones Bridge Rd., Chevy Chase, MD 20815, USA

Abstract

A major limitation of cell therapies is the rapid decline in viability and function of transplanted cells. Here we describe a strategy to enhance cell therapy via the conjugation of adjuvant drug-loaded nanoparticles to the surfaces of therapeutic cells. Using this method to provide sustained pseudo-autocrine stimulation to donor cells, we elicited dramatic enhancements in tumor elimination in a model of adoptive T-cell therapy for cancer and increased the *in vivo* repopulation rate of hematopoietic stem cell grafts, using very low doses of adjuvant drugs that were ineffective when given systemically. This approach is a facile and generalizable strategy to augment cytoreagents while minimizing systemic side effects of adjuvant drugs. In addition, these results suggest therapeutic cells are promising vectors for actively targeted drug delivery.

Cell-based therapies, such as hematopoietic stem cell (HSC), islet cell, or hepatocyte transplants are in routine clinical practice[1],[2], while new treatment strategies implementing adult, embryonic, or induced pluripotent stem cells are in various stages of development[3],[4]. In the field of cancer immunotherapy, early clinical trials infusing *ex vivo*-expanded tumor-specific T-lymphocytes have yielded promising results for the treatment of cancer and chronic infections[5]-[7]. Notably, following cell transfer, therapeutic cells often rely on the co-

‡ To whom correspondence should be addressed. djirvine@mit.edu.

Author Contributions: M.T.S. designed and conducted all experiments and wrote the manuscript. J.J.M. assisted in T-cell transmigration assays, optimization of multilamellar lipid NP synthesis, and *in vivo* NP biodistribution assays. S.H.U. assisted optimization of multilamellar lipid NP synthesis. A.B. assisted in initial *in vitro* T cell assays, collected electron microscopy images, and contributed experimental suggestions. D.J.I. supervised all experiments and wrote the manuscript.

Competing financial interest: The authors declare no competing financial interests.

delivery of adjuvant drugs. These agents are designed to maximize donor cell efficacy and *in vivo* persistence, offset suppressive molecules at cell homing sites, or promote the differentiation of transferred cells into a therapeutically optimal phenotype. Examples include γ_c receptor cytokines[5,8] or TGF-β signaling inhibitors[9] in adoptive T-cell therapy, or the use of small-molecule drugs to boost immune reconstitution following HSC transplants[10]. However, these agents often require high and sustained systemic levels for efficacy. This leads to dose-limiting toxicities for these drugs due to their generally pleiotropic activity, which has restricted their clinical use[11,12]. One approach to focus adjuvant drug action on the transferred cells is to genetically engineer donor cells to secrete their own supporting factors[13]. However, regulatory and cost barriers of large-scale clinical grade vector production and safety testing, costly and lengthy cell culture, and technical challenges of efficient gene transfer hinder the implementation of clinical gene therapy protocols. More importantly, several emerging adjuvant therapies are based on small-molecule drugs that cannot be genetically encoded[9,10]. Here we describe an alternate strategy for adjuvant drug delivery in cell therapies, based on chemical conjugation of submicron-sized drug-loaded synthetic particles directly onto the plasma membrane of donor cells, enabling continuous pseudo-autocrine stimulation of transferred cells *in vivo*.

Results

Stable nanoparticle (NP) attachment to cell surfaces

To stably couple synthetic drug carrier NPs to the surface of therapeutic cells, we exploited the fact that many cells exhibit high levels of reduced thiol groups on their surfaces[14]. Confirming prior reports, we detected substantial levels of free thiols on the surfaces of T-cells, B-cells, and HSCs, but low amounts on red blood cells (Fig. 1a). To link synthetic drug carriers to cells using these surface thiols, we utilized liposomes and liposome-like synthetic NPs 100-300 nm in diameter with a drug-loaded core and phospholipid surface layer, where the lipid bilayer surface of the particles included thiol-reactive maleimide headgroups (Supplementary Fig. 1). We achieved particle conjugation by a simple two-step process (Fig. 1b): donor cells were first incubated with NPs to permit maleimide-thiol coupling, followed by *in situ* PEGylation with thiol-terminated poly(ethylene glycol) (PEG) to quench residual reactive groups of the particles (Supplementary Fig. 2). With this approach, we could covalently link a substantial number of NPs with diameters in the 100-300 nm range to cell types used commonly in cell therapy, including $CD8^+$ T lymphocytes or $lineage^-Sca\text{-}1^+c\text{-}kit^+$ HSCs (Fig. 1c, left panels). Particles ranging from simple liposomes (with an aqueous drug-loaded core), to more complex multilamellar lipid NPs or lipid-coated polymer NPs[15] (Fig. 1c, and Supplementary Figs. 1 and 3) were stably attached to live cells. Importantly, particle coupling was benign; coupling of up to 140 (±30) ~200 nm-diameter multilamellar lipid NPs to the surface of cells was nontoxic (Supplementary Fig. 4), and blocked only 17.2% (± 8.7%) of the total available cell surface thiol groups (Supplementary Fig. 5). These findings are consistent with a simple calculation of the surface area occupied by the NPs: attachment of 150 particles each 200 nm in diameter would occlude only 3% of the surface of a typical 7 μm-diameter T-cell. Although liposomes and lipid-coated polymer particles spontaneously adsorbed to cell surfaces, we found that physically-adsorbed particles were removed during mild cell washing steps, while

maleimide-linked particles remained stably bound to cells (Fig. 1d). Attachment of NPs to T-cells did not trigger spontaneous activation of the cells (Supplementary Fig. 6), and strikingly, particles bound to lymphocytes or HSCs remained localized at the cell surface as revealed by optical sectioning with confocal microscopy (Fig. 1c, and Supplementary Movies 1 and 2), and by flow cytometry internalization assays (Fig. 1e), even following extended *in vitro* stimulation (Fig. 1c, right panels). In contrast, we observed that phagocytic cells such as immature dendritic cells efficiently internalized maleimide-functionalized NPs after a short incubation (Fig. 1e). Although all three types of NPs tested here conjugated to lymphocytes with comparable efficiency, we chose to focus on ∼300 nm-diameter multilamellar lipid NPs (Supplementary Fig. 1b) for our subsequent *in vitro* functional and *in vivo* therapeutic studies, based on their high drug encapsulation efficiencies, week-long drug release profiles, and the lack of inflammatory responses elicited from innate immune cells exposed to the “empty” particles (Supplementary Figs. 7 and 8).

NP conjugation does not compromise key cellular functions

We next determined the maximal number of particles (without encapsulated drug cargo) that could be linked to cells without compromising key cellular functions, focusing on therapeutic cytotoxic T-cells that must be capable of forming an immunological synapse and killing target cells, proliferating, and secreting cytokines as part of their normal function. TCR-transgenic OT-1 $CD8^+$ T-cells conjugated with up to 100 (±20) NPs per cell retained an unmodified proliferative response after co-culture with ovalbumin-pulsed dendritic cells; higher surface densities of particles began to inhibit T-cell proliferation (Fig. 2a, and Supplementary Fig. 9a,b). During cell division, surface-attached NPs segregated equally to daughter cells, reflected by a stepwise decrease in the mean fluorescence from cell-conjugated NPs with increasing number of divisions (Figs. 1c and 2a). Attachment of at least ∼100 particles/cell also did not impact T-cell recognition/killing of ovalbumin peptide-pulsed target cells or cytokine release profiles (Fig. 2b, and Supplementary Figure 9c). We next assessed the impact of cell surface-tethered NPs on T-cell transmigration across endothelial monolayers – a key capability of any therapeutic cell to efficiently infiltrate its target tissue. We first utilized an *in vitro* transwell co-culture system and quantified the migration of NP-conjugated T-lymphocytes across a membrane-supported confluent endothelial monolayer in response to a chemoattractant placed in the lower chamber. T-cells carrying 100 NPs/cell exhibited unaltered transmigration efficiencies compared to unmodified cells (Fig. 2c). After crossing the endothelial barrier, T-cells retained 83% (±3%) of their original NP cargo physically attached (Fig. 2d). (In comparative experiments, liposomes and lipid-coated PLGA particles could also be carried through endothelial layers by T-cells, though PLGA particles were not retained as well by transmigrating cells and showed a tendency to inhibit T-cell transmigration at high particle/cell loadings, Supplementary Fig. 10)

To determine whether *in vivo* tissue homing of T-cells was affected by NP conjugation, we evaluated the tumor-homing properties of particle-conjugated lymphocytes. Subcutaneous EL4 tumors expressing membrane-bound Gaussia luciferase (extG-luc) and ovalbumin (EG7-OVA) or exG-luc alone were established on opposite flanks of C57Bl/6 mice. Tumor-bearing mice then received adoptive transfers of Firefly luciferase (F-luc)-transgenic OT-1

T-cells with or without surface-conjugated red-fluorescent NPs, or an i.v. injection of an equivalent dose of fluorescent particles alone. Particle-carrying OT-1 T-cells specifically trafficked to EL4-OVA tumors (Fig. 3a), and no difference in the tumor homing potential of particle-conjugated compared to unmodified OT-1 T-cells was observed (Fig. 3b, upper panel). Quantitative fluorescent particle imaging of EG7-OVA tumors demonstrated that NPs accumulated a mean 176-fold more efficiently at the tumor site when surface-attached to OT-1 T-cells compared to systemically infused free NPs, which were rapidly scavenged by the liver and the spleen (Fig. 3b,d). Flow cytometry analysis independently verified that T-cell infiltration of EG7-OVA tumors was quantitatively identical for particle-decorated and control OT-1 cells, and that the majority of particle-conjugated cells recovered from tumors still retained their NP cargo (Fig. 3a). In separate experiments using fluorescently-labeled OT-1 T-cells, we confirmed prominent infiltration of NP-decorated T-cells into EG7-OVA tumors in histological tumor sections examined by confocal microscopy, and NPs appeared surface-localized as observed *in vitro* (Fig. 3c, Supplementary Fig. 11, Supplementary Movie 3,4). Of note, the ability of lymphocytes to efficiently transfer surface-tethered NPs across endothelial barriers *in vivo* was not restricted to the abnormal endothelial lining[16] found in tumor vasculature. When we linked particles to resting $CCR7^{+}CD62L^{+}$ B-cells (Supplementary Fig. 12) or central memory $CD8^{+}$ T-cells (data not shown), particles were transported across the intercellular boundaries of high endothelial venules into lymph nodes – a poorly accessible compartment for systemically infused free NPs.

Cell-Bound NPs enhance cytokine support of anti-tumor T-cells

We next tested whether cell-bound adjuvant drug-loaded NPs could directly impart amplified therapeutic functions to their cellular carriers, using self/tumor-reactive $CD8^{+}$ T-cell receptor transgenic Pmel-1 melanoma-specific T-cells to treat established, disseminated B16F10 melanoma lung and bone marrow mestastases[17]. We encapsulated a mixture of the cytokines IL-15 (converted to a superagonist (IL-15Sa) by pre-complexing with soluble IL-15Rα[18]) and IL-21 into multilamellar lipid NPs. These two interleukins cooperatively promote *in vivo* T-cell expansion and effector function when administered daily at high doses[8]. Particles ∼300 nm in diam. efficiently entrapped IL-15Sa and IL-21 and released bioactive cytokine over a seven-day period (Supplementary Fig. 13). These cytokine-loaded particles were conjugated to Click bettle red (CBR)-luciferase expressing $CD8^{+}$ Pmel-1 effector T-cells. Particle-conjugated or control T-cells were infused into lymphodepleted mice bearing established Gaussia luciferase-expressing B16F10 melanoma lung and bone marrow tumors (Fig. 4a). Serial imaging of non-adjuvanted Pmel-1 T-cells showed a gradual CBR-luc signal decline following T-cell injection, consistent with poor *in vivo* T-cell expansion and persistence (Fig. 4a–c). Whereas a single systemic infusion of 5 μg free cytokine (4.03 μg IL-15Sa + 0.93 μg IL-21) given on the day of adoptive transfer did not significantly boost Pmel-1 proliferation (1.4-fold-higher CBR-luc signal on day 6, $P = 0.32$), the same cytokine dose loaded in cell-bound NPs elicited markedly amplified proliferation by Pmel-1 cells (81-fold higher peak photon count relative to unmodified Pmel-1 T-cells on day 6, $P < 0.0001$, Fig. 4a,c). Subsequent to a contraction period, cytokine NP-carrying T-cells displayed enhanced long-term persistence (14.8-fold and 4.7-fold higher photon counts than Pmel-1 T-cells alone at 16 and 30 days after T-cell infusion, respectively, $P < 0.0001$)

and homed as $CD44^+CD62L^+$ central memory T-cells to lymph nodes and spleen (Fig. 4a,b, and Supplementary Fig. 14). Notably, experiments comparing the *in vivo* proliferative response of T-cells bearing cytokine-loaded NPs vs. bystander tumor-homing T-cells showed that NP-released cytokines activated T-cells primarily in *cis* with limited paracrine stimulation of bystander cells (Supplementary Fig. 15). The adjuvant effect of T-cell-conjugated cytokine NPs was largely tumor antigen-independent (Supplementary Fig. 16b,d), consistent with earlier studies demonstrating antigen-independent proliferation of T-cells in response to IL-15,[19] but there was no evidence of progressive T-cell clonality or leukemia formation in any treated animal imaged at late time points (data not shown). Importantly, cytokine-loaded particles co-injected but not attached to T-cells elicited a 4.9-fold higher peak Pmel-1 T-cell proliferation compared to the same cytokine dose administered in a non-encapsulated soluble form (day 6, $P = 0.0052$), but this stimulatory effect was still 11-fold ($P < 0.0001$) less than that obtained by linking the same number of cytokine-loaded NPs directly to the surface of the adoptively transferred T-cells (Supplementary Fig. 16c,d). Pmel-1 T-cells conjugated with “empty” NPs exhibited the same expansion/decline *in vivo* as unmodified Pmel-1 cells (Supplementary Figure 16a,d). All mice receiving cytokine NP-decorated Pmel-1 T-cells achieved complete tumor clearance (Fig. 4a,d), whereas treatment with Pmel-1 T-cells with or without systemic cytokine infusion at the same doses yielded only modest survival advantages (Fig. 4a,d). The *in vivo* tumor eradication potential of cytokine NP-conjugated Pmel-1 T lymphocytes was also investigated in animals bearing large, established subcutaneous B16F10 flank tumors. Animals treated with unmodified Pmel-1 T-lymphocytes uniformly succumbed to tumors within 30 d, whereas the infusion of cytokine NP-decorated Pmel-1 T-cells prevented tumor growth, with all animals alive 30 d after T-cell treatment (Supplementary Fig. 17).

Enhanced HSC reconstitution via cell-bound adjuvant NPs

Prompted by the substantial therapeutic benefits achieved with conjugation of cytokine-loaded particles to tumor-specific T-cells, we further examined the utility of this new adjuvant delivery approach in the context of hematopoietic stem cell transplantations. We chose the glycogen synthase kinase-3 β (GSK-3β) inhibitor TWS119[20] as therapeutic cargo, based on reports that repeated high-dose bolus therapy of transplant recipients with glycogen synthase kinase-3 (GSK-3) inhibitors enhances the repopulation kinetics of donor HSCs[10]. Multilamellar lipid nanoparticles efficiently encapsulated this small-molecule drug, and slowly released it over a seven-day time window (Supplementary Fig. 13). We evaluated the *in vivo* repopulation capabilities of hematopoietic grafts supported by cell-bound TWS119-loaded NPs based on the whole body photon emission from Firefly luciferase-transgenic donor HSCs, and in separate experiments, by tracing the frequencies of GFP^+ donor HSCs by flow cytometry. Following transplantation of $lineage^-Sca\text{-}1^+c\text{-}kit^+$ HSCs from luciferase-transgenic donors into lethally-irradiated syngeneic recipients, a steady increase in whole body bioluminescent emission was observed originating from discrete foci over anatomic sites corresponding to the femurs, humeri, sternum and the spleen (Fig. 5a). Whereas a systemic TWS119 bolus injection (1.6 ng) at the time of transplantation did not significantly alter measured engraftment kinetics (Fig. 5a,b), the same TWS119 dose encapsulated in NPs surface-tethered to donor HSCs markedly enhanced reconstitution by HSC grafts (median

5.7-fold higher bioluminescence than systemic TWS119 after one week, $P < 0.0001$, Fig. 5a–c). Notably, animals in all treatment groups initially engrafted HSCs in both femurs and the sternum, indicating that NP conjugation did not compromise the intrinsic homing properties of donor HSCs. While increasing the rate of initial reconstitution, conjugating TWS119 NPs onto HSCs did not affect their multilineage differentiation potential, reflected by a similar frequency of donor-derived GFP^+ reconstituted cell types compared to control HSC grafts three months after transplantation (Fig. 5d). Thus, this simple approach for donor cell modification just prior to cell transfer can also augment hematopoietic stem cell transplants, a procedure in routine clinical practice.

Discussion

Cell therapies are in common clinical practice for certain indications (e.g., HSC and islet cell transplants) and are also being aggressively developed in other areas of medicine, such as adoptive T-cell therapy of cancer[5-7]. However, many cell therapy protocols rely on adjuvant drugs that act directly on the transferred therapeutic cells to maintain their function, phenotype, and/or lifespan. A ubiquitous challenge is the pleiotropic activity of many biological and small-molecule drugs, leading to toxicity or unwanted side effects following systemic exposure. This problem is illustrated by the use of interleukin-2 in the support of adoptive T-cell therapy of melanoma, where IL-2 provides important adjuvant signals to donor T-cells, but also elicits severe dose-limiting toxicity[12].

Here, we devised a facile and generalizable strategy to robustly augment the therapeutic potential of cytoreagents, while limiting the potential for side effects from adjuvant drugs. We showed that adjuvant agent-releasing particles can be stably conjugated to cells without toxicity or interference with intrinsic cell functions, follow the characteristic *in vivo* migration patterns of their cellular vehicles and, ultimately, endow their carrier cells with substantially enhanced function using low drug doses that have no effect when given by traditional systemic routes. Prolonged retention of the particles on the surfaces of donor cells as shown here enables sustained drug release without concerns of premature degradation of the particle carrier or cargo due to internalization into degradative intracellular compartments. Notably, prior work has shown that particles ∼200 nm in diameter coated with anti-CD3 are readily internalized by T-cell lines[21], suggesting that internalization of particles in the size range studied here is not impossible for lymphocytes *per se*, but rather that internalization may be tightly regulated at the cell surface– elucidating the mechanism(s) for prolonged particle retention on T-cell and HSC surfaces is an area for future study. Numerous reports have illustrated the potential of systemically-infused nanoparticle materials slowly releasing drug cargos to enhance the efficacy of therapeutic drugs, and this has led to the development of clinical products such as anthracycline-loaded liposomes for cancer therapy[22]. However, in the context of support for cell therapy, our data demonstrate that conjugation of drug-loaded particles directly to the donor cells increases their therapeutic impact significantly (here, ∼10-fold increases in peak T-cell expansion in an adoptive T-cell therapy model for particles attached to cells vs. the same particles systemically infused). This strategy does not require cell preconditioning and complements traditional genetic engineering or chemical biology approaches[23] to augment or reprogram cell function. Based on the wealth of available nanoparticle formulations tailored to deliver

small molecule drugs, proteins, siRNA, or magnetic imaging agents[24-27], the range of therapeutic or diagnostic cargos that can be attached to therapeutic cells likely extends far beyond the small molecules and recombinant proteins illustrated here.

Our study further demonstrates the concept of cells as chaperones that actively direct drug-loaded nanoparticles into poorly accessible anatomical compartments. In the field of cancer therapy, targeting strategies functionalizing drugs or biomaterials with specific tumor-targeting ligands, such as antibodies, aptamers, small molecules or folic acid have been demonstrated to improve therapeutic efficacy[28-30]. However, these approaches generally rely on the initially passive accumulation of targeted therapeutics at tumor sites via the enhanced permeation and retention effect[27], and it has been shown in some systems that targeting ligands do not change the overall tissue biodistribution of i.v.-delivered nanoparticle drug carriers, but rather enable those particles that do reach tumors to be more efficiently internalized by target cells[28,31]. In contrast, cellular nanoparticle vectors actively transmigrate the endothelial barrier and accumulate cell-attached cargo in tissues at >100-fold greater levels than systemically infused free particles. This profoundly altered biodistribution opens new venues, beyond existing cell therapies, for applications of cell products as actively targeting drug delivery “pharmacytes” or vaccine delivery tools.

Methods

Cell lines

The murine melanoma cell line B16F10, the pancreatic islet endothelial cell line MS1, the thymoma cell line EL4 and EG7-OVA, an EL4 cell line stably transfected with the plasmid pAc-neo-OVA which carries a complete copy of chicken ovalbumin (OVA) mRNA, were all purchased from the American Type Culture Collection (ATCC). We purchased the Phoenix™ Eco retroviral packaging cell line from Orbigen. For bioluminescent in vivo tumor imaging we retrovirally transduced the B16F10, EL4 and EG7-OVA cell lines with a membrane-anchored form of the *Gaussia* luciferase (extG-Luc), provided to us by M. Sadelain (Memorial Sloan-Kettering Cancer Center), as described in the Supplementary Methods.

Mice and *in vivo* tumor models

Animals were housed in the MIT Animal Facility. We performed all mouse studies in the context of an animal protocol approved by the MIT Division of Comparative Medicine following federal, state, and local guidelines. C57Bl/6 mice, C57Bl/6-Pmel-1-Thy1.1 mice, OT-1 OVA-TCR transgenic mice, and C57Bl/6-GFP-transgenic mice were all obtained from Jackson Laboratories. C57Bl/6 (H-2K^b, Thy-1.1) firefly luciferase (F-luc)-transgenic mice [32] were provided to us by M. van den Brink (Memorial Sloan-Kettering Cancer Center). For adoptive T-cell experiments with OVA-specific transgenic T cells, we subcutaneously injected C57Bl/6 mice with 4×10^6 EG7-OVA tumor cells into the right flank and 2×10^6 control EL4 cells into the left flank to generate equally sized s.c. tumors seven days later. We retrovirally transduced both tumor cell lines with extG-luc for bioluminescent imaging. To establish melanoma lung tumor metastases, we injected 1×10^6 B16F10-extG-luc tumor cells i.v. via the tail vein into C57Bl/6 mice one week before T cell treatment. On the day of

adoptive Pmel-1 T cell transfer, we sublethally irradiated recipient mice with 500 cGy of total body irradiation from a ^{137}Cs source. All mice were treated with a single infusion of 15 × 10^6 effector $CD8^+$ T cells.

Preparation of primed T-cells for adoptive transfer and retroviral transduction

Spleens were harvested, macerated over a filter, and resuspended in ACK lysing Buffer (Biosource, Rockville, MD). In all, we placed 3 × 10^6 splenocytes per milliliter in complete RPMI 1640 with 1 ng mL^{-1} IL-7 and 2 μg mL^{-1} Concavalin A (Calbiochem, La Jolla, CA), and incubated at 37°C. Two days later, we removed dead cells by Ficoll gradient (GE Healthcare) and isolated $CD8^+$ cells using a mouse CD8 Negative Isolation Kit (Stemcell Technologies). We then preloaded 1 mL per well of concentrated retrovirus (see Supplementary Methods) on six-well non-tissue culture treated dishes coated with RetroNectin (TakiraBio) and incubated them at 37°C incubation for 1 h. An equal volume of isolated T cells (3 × 10^6 cells mL^{-1} substituted with 50 IU hIL-2 mL^{-1}) was added and centrifuged at 2000 × g for 30 min. 6 h after spinoculation, 1 mL of fresh, prewarmed RPMI, containing 50 IU hIL-2 (Chiron) was added. We used T cells for adoptive transfer experiments one day after gene transfer.

NP conjugation with cells and *in situ* PEGylation

Detailed information on nanoparticle and liposome synthesis as well as cytokine/small molecule particle loading is included in the Supplementary Methods. We resuspended 60 × 10^6 cells mL^{-1} in serum-free X-Vivo 10 medium (Cambrex) following two PBS washes. We then added an equal volume of NPs in nuclease-free water, with 1200/600/300/or 150 NPs/T cell (resulting in 139±29/128±23/100±21 or 75±32 surface-tethered particles/T-cell, respectively, after cell washes and PEGylation), and incubated at 37°C for 30 min with gentle agitation every 10 min. After a PBS wash to separate cells from unbound particles, we quenched residual maleimide groups present on cell-bound particles by incubation of 3 × 10^6 cells mL^{-1} with 1 mg mL^{-1} thiol-terminated 2Kda poly(ethylene glycol) (PEG, Laysan Bio) at 37°C for 30 min in complete RPMI medium, followed by 2 PBS washes to remove unbound PEG.

We determined 1 mg mL^{-1} thiol-PEG as the optimal concentration required to quench all remaining maleimide groups displayed on NPs after cell conjugation based on no significant FACS signal following a 30 min incubation with 70 mg ml^{-1} bodipy-tagged cysteine (generated from reduction of disulfide bond in bodipy L-cystine (Invitrogen; Carlsbad, CA) with 15 molar excess of TCEP (Thermo Scientific; Rockford, IL) for 45 min at RT). The nanoparticle binding efficiency of maleimide-functionalized (50 mole% maleimide MPB-PE in the lipid fraction) multilamellar lipid NPs to effector T lymphocytes was 33.4% (± 6.9%), when incubating 500 particles/T-cell, as determined by high magnification confocal microscopy imaging of 30 single T cell z-stacks. We distinguished between surface-conjugated and internalized NPs from by flow cytometry internalization assay, described in the Supplementary Methods.

Functional in vitro T-cell and HSC assays, HSC transplantation, *in vivo* bioluminescence and fluorescence imaging, NP biodistribution assay, flow cytometry and confocal microscopy

Detailed information on in vitro T cell and HSC assay, transplantation, serial bioluminescent imaging and confocal microscopy assays are included in the Supplementary Methods.

Supplementary Material

Refer to Web version on PubMed Central for supplementary material.

Acknowledgments

This work was supported in part by the National Institute of Health (CA140476), the National Science Foundation (MRSEC award DMR-02-13282), Cancer Center Support (core) grant P30-CA14051 from the National Cancer Institute, and a gift to the Koch Institute by Curtis and Cathy Marble. DJI is an investigator of the Howard Hughes Medical Institute.

References

1. Fiorina P, Shapiro AM, Ricordi C, Secchi A. The clinical impact of islet transplantation. Am J Transplant. 2008; 8:1990–1997. [PubMed: 18828765]
2. Alison MR, Islam S, Lim SM. Cell therapy for liver disease. Current opinion in molecular therapeutics. 2009; 11:364–374. [PubMed: 19649981]
3. Alper J. Geron gets green light for human trial of ES cell-derived product. Nature biotechnology. 2009; 27:213–214.
4. Dimos JT, et al. Induced pluripotent stem cells generated from patients with ALS can bedifferentiated into motor neurons. Science (New York N Y. 2008; 321:1218–1221.
5. Morgan RA, et al. Cancer regression in patients after transfer of genetically engineeredlymphocytes. Science (New York N Y. 2006; 314:126–129.
6. Hunder NN, et al. Treatment of metastatic melanoma with autologous CD4+ T cells against NY-ESO-1. N Engl J Med. 2008; 358:2698–2703. [PubMed: 18565862]
7. Mackinnon S, Thomson K, Verfuerth S, Peggs K, Lowdell M. Adoptive cellular therapy for cytomegalovirus infection following allogeneic stem cell transplantation using virus-specific T cells. Blood cells, molecules & diseases. 2008; 40:63–67.
8. Zeng R, et al. Synergy of IL-21 and IL-15 in regulating CD8+ T cell expansion and function. J Exp Med. 2005; 201:139–148. [PubMed: 15630141]
9. Wallace A, et al. Transforming growth factor-beta receptor blockade augments the effectiveness of adoptive T-cell therapy of established solid cancers. Clin Cancer Res. 2008; 14:3966–3974. [PubMed: 18559619]
10. Trowbridge JJ, Xenocostas A, Moon RT, Bhatia M. Glycogen synthase kinase-3 is an in vivo regulator of hematopoietic stem cell repopulation. Nat Med. 2006; 12:89–98. [PubMed: 16341242]
11. Berger C, et al. Safety and immunological effects of IL-15 administration in nonhuman primates. Blood. 2009
12. Thompson JA, et al. Recombinant interleukin 2 toxicity, pharmacokinetics, and immunomodulatory effects in a phase I trial. Cancer Res. 1987; 47:4202–4207. [PubMed: 3496957]
13. Treisman J, et al. Interleukin-2-transduced lymphocytes grow in an autocrine fashion and remain responsive to antigen. Blood. 1995; 85:139–145. [PubMed: 7803791]
14. Sahaf B, Heydari K, Herzenberg LA, Herzenberg LA. Lymphocyte surface thiol levels. Proc Natl Acad Sci U S A. 2003; 100:4001–4005. [PubMed: 12642656]
15. Bernstein ID, Boyd RL, van den Brink MR. Clinical strategies to enhance posttransplant immune reconstitution. Biol Blood Marrow Transplant. 2008; 14:94–99. [PubMed: 18162228]

16. Jain RK. A new target for tumor therapy. N Engl J Med. 2009; 360:2669–2671. [PubMed: 19535806]
17. Overwijk WW, et al. gp100/pmel 17 is a murine tumor rejection antigen: induction of “self”-reactive, tumoricidal T cells using high-affinity, altered peptide ligand. J Exp Med. 1998; 188:277–286. [PubMed: 9670040]
18. Rubinstein MP, et al. Converting IL-15 to a superagonist by binding to soluble IL-15R{alpha}. Proc Natl Acad Sci U S A. 2006; 103:9166–9171. [PubMed: 16757567]
19. Lu J, et al. Interleukin 15 promotes antigen-independent in vitro expansion and long-term survival of antitumor cytotoxic T lymphocytes. Clin Cancer Res. 2002; 8:3877–3884. [PubMed: 12473603]
20. Gattinoni L, et al. Wnt signaling arrests effector T cell differentiation and generates CD8+ memory stem cells. Nat Med. 2009; 15:808–813. [PubMed: 19525962]
21. Dinauer N, et al. Selective targeting of antibody-conjugated nanoparticles to leukemic cells and primary T-lymphocytes. Biomaterials. 2005; 26:5898–5906. [PubMed: 15949555]
22. Davis ME, Chen ZG, Shin DM. Nanoparticle therapeutics: an emerging treatment modality for cancer. Nature reviews. 2008; 7:771–782.
23. Prescher JA, Dube DH, Bertozzi CR. Chemical remodelling of cell surfaces in living animals. Nature. 2004; 430:873–877. [PubMed: 15318217]
24. Reddy ST, et al. Exploiting lymphatic transport and complement activation in nanoparticle vaccines. Nat Biotechnol. 2007; 25:1159–1164. [PubMed: 17873867]
25. Woodrow KA, et al. Intravaginal gene silencing using biodegradable polymer nanoparticles densely loaded with small-interfering RNA. Nat Mater. 2009; 8:526–533. [PubMed: 19404239]
26. Na, Hyon Bin; S, IC.; Hyeon, Taeghwan. Inorganic Nanoparticles for MRI Contrast Agents. Advanced Materials. 2009; 21:16.
27. Tong R, C DA, Tang L, Cabral H, Baker JR Jr, Kataoka K, Discher D, Cheng J. Nanopolymeric Therapeutics. MRS Bulletin. 2009; 34:422–431.
28. Bartlett DW, Su H, Hildebrandt IJ, Weber WA, Davis ME. Impact of tumor-specific targeting on the biodistribution and efficacy of siRNA nanoparticles measured by multimodality in vivo imaging. Proc Natl Acad Sci U S A. 2007; 104:15549–15554. [PubMed: 17875985]
29. Weissleder R, Kelly K, Sun EY, Shtatland T, Josephson L. Cell-specific targeting of nanoparticles by multivalent attachment of small molecules. Nat Biotechnol. 2005; 23:1418–1423. [PubMed: 16244656]
30. Dhar S, Gu FX, Langer R, Farokhzad OC, Lippard SJ. Targeted delivery of cisplatin to prostate cancer cells by aptamer functionalized Pt(IV) prodrug-PLGA-PEG nanoparticles. Proc Natl Acad Sci U S A. 2008; 105:17356–17361. [PubMed: 18978032]
31. Kirpotin DB, et al. Antibody targeting of long-circulating lipidic nanoparticles does not increase tumor localization but does increase internalization in animal models. Cancer Res. 2006; 66:6732–6740. [PubMed: 16818648]
32. Reichardt W, et al. Impact of mammalian target of rapamycin inhibition on lymphoid homing and tolerogenic function of nanoparticle-labeled dendritic cells following allogeneic hematopoietic cell transplantation. J Immunol. 2008; 181:4770–4779. [PubMed: 18802080]

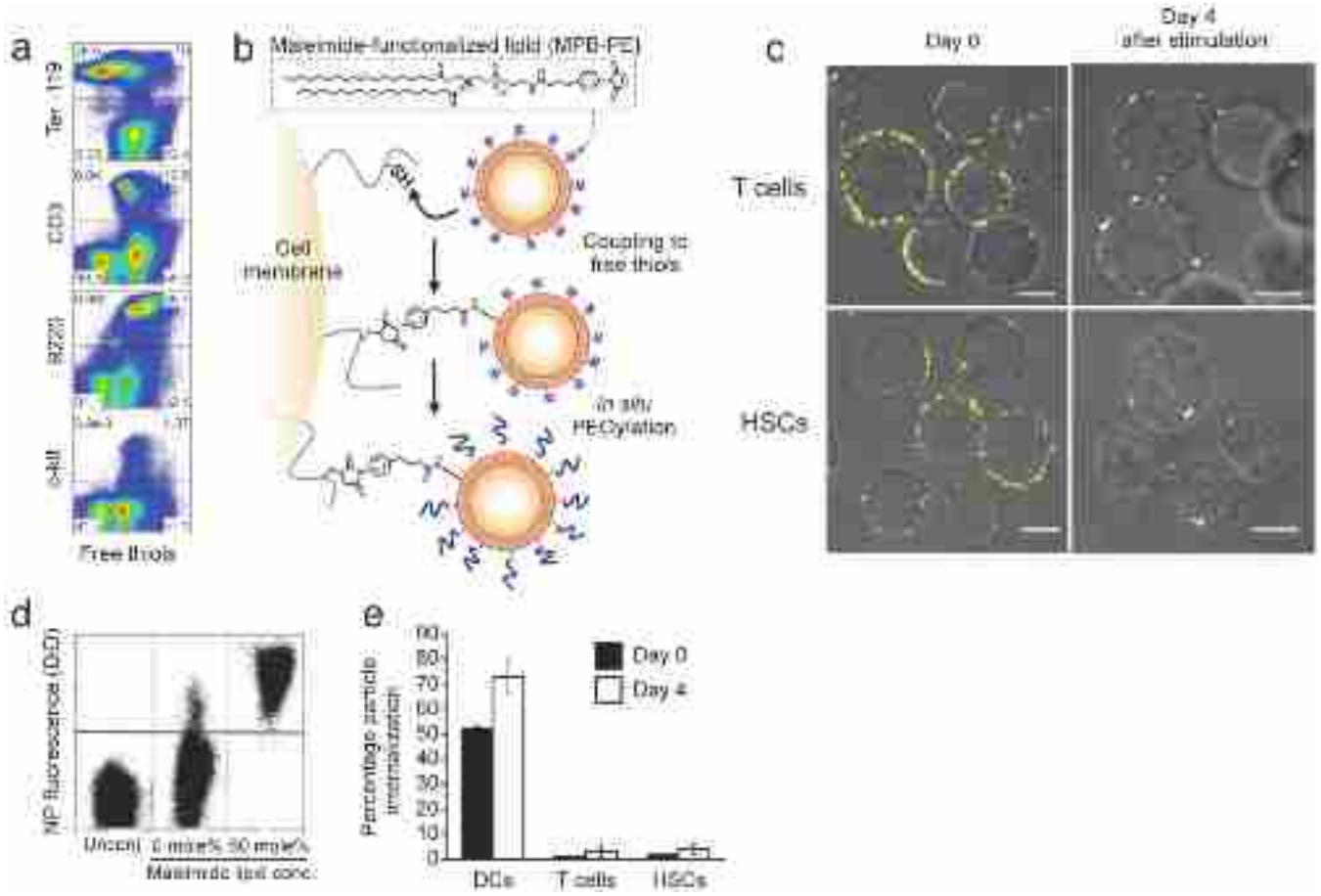

Figure 1.

Stable conjugation of nanoparticles (NPs) to the surfaces of T-cells and HSCs via cell-surface thiols. (**a**) Flow cytometry analysis of cell surface thiols on mouse splenocytes detected by fluorophore-conjugated malemide co-staining with lineage surface markers for erythrocytes (Ter-119), T-cells (CD3), B-cells (B220) and hematopoietic stem cells (c-kit). (**b**) Schematic of maleimide-based conjugation to cell surface thiols. (**c**) Confocal microscopy images of $CD8^+$ effector T-cells and $lineage^-Sca\text{-}1^+c\text{-}kit^+$ HSCs immediately following conjugation with fluorescent DiD-labeled multilamellar lipid NPs (left panel) and after four day *in vitro* expansion (right panel). Scale bars, 2 μm. (**d**) Flow cytometry analysis of $CD8^+$ T-cells after incubation with DiD-labeled multilamellar lipid NPs synthesized with or without maleimide-headgroup lipids. (**e**) Quantification of nanoparticle internalization. Immature dendritic cells (DCs), effector $CD8^+$ T-cells, or HSCs were conjugated with carboxyfluorescein-tagged maleimide-bearing liposomes. Extracellular trypan blue quenching was used to differentiate surface-bound and internalized liposomes immediately following conjugation or after four days in culture.

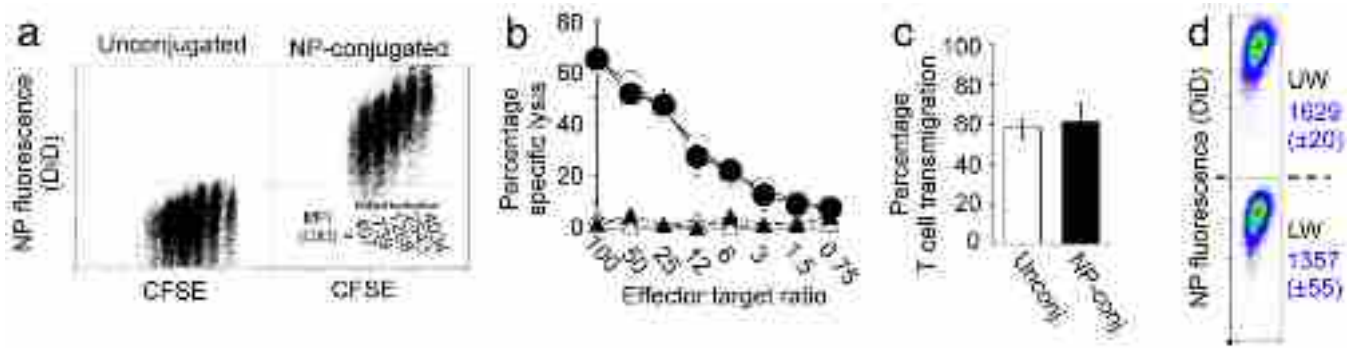

Figure 2.

Nanoparticle conjugation does not impact key T-cell functions. OT-1 ova-specific $CD8^+$ effector T-cells were conjugated with 100 DiD-labeled multilamellar lipid NPs per cell or left unmanipulated as controls. (**a**) CFSE dilution of unmodified or NP-conjugated T-cells stimulated *in vitro* with mature ova peptide-pulsed dendritic cells. DiD Mean Fluorescence Intensities (MFI) for distinct CFSE lymphocytes populations are indicated on the right. (**b**) Standard 4 h ^{51}Cr release assay comparing cytotoxicity of unmanipulated (open symbols) and particle-conjugated (filled symbols) OT-1 cells targeting ova peptide-pulsed (circles) or control (triangles) EL4 tumor cells. (**c**,**d**) Transmigration of OT-1 T-cells (with or without surface-bound particles) seeded onto MS1 endothelial cell monolayers in the upper well of a transwell chamber, following addition of the chemoattractant MCP-1 to the lower chamber. The fraction of transmigrating T-cells (**c**) and the profile of cell-bound NP fluorescence before (UW) and after (LW) transmigration (**d**) were quantitated by flow cytometry. (DiD MFI±s.e.m. from triplicate samples shown in blue).

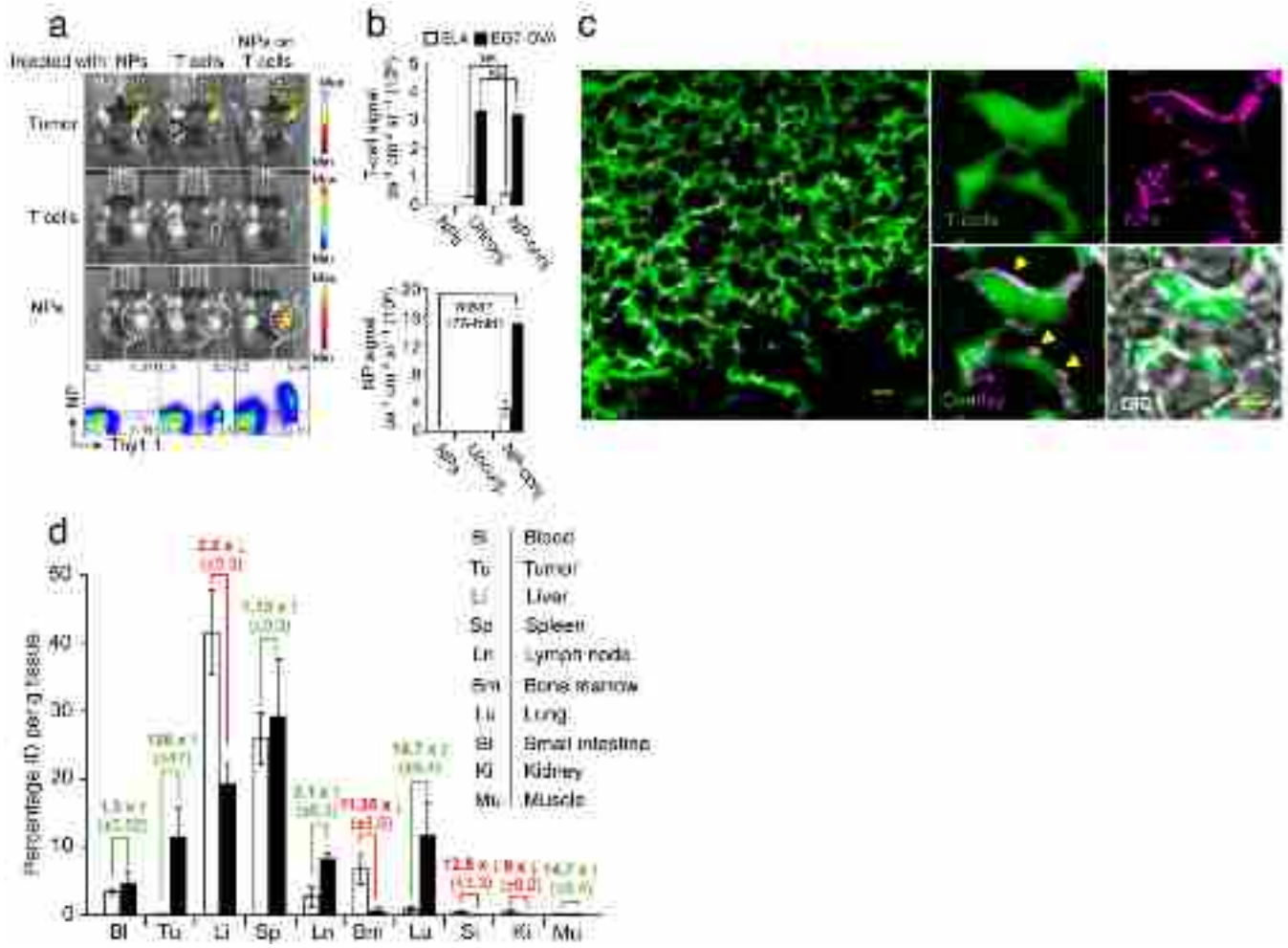

Figure 3.

Nanoparticle-decorated T cells efficiently carry surface-tethered NPs into antigen-expressing tumors. (**a**,**b**) Comparative whole-animal *in vivo* bioluminescence (tumors, T-cells) and fluorescence imaging (NPs) of mice bearing established s.c. Gaussia luc-expressing EG7-OVA and EL4 tumors on opposite flanks, two days after i.v. infusion of firefly luc-transgenic Thy1.1^{+} effector OT-1 T-cells (with or without attached DiD-labeled NPs), or an equivalent number of free NPs. Thy1.1^{+} OT-1 T-cells recovered from the EG7-OVA tumors were analyzed for surface-bound DiD NPs by flow cytometry (**a**), and the mean bioluminescent T-cell and fluorescent NP signals from groups of 6 mice are shown in (**b**). NS, no significance. (**c**) In an independent experiment, CellTracker green-labeled OT-1 T-cells conjugated with rhodamine-labeled NPs were transferred into mice bearing established s.c. EG7-OVA tumors, and tumors were excised and sectioned for confocal histological analysis two days later. Scale bar, 10 μm. A higher magnification image of NP-carrying tumor infiltrating T-cells is shown in the right panel. Scale bar, 1.5 μm. Yellow arrowheads highlight evidence for surface localization of NPs. Shown is 1 of 2 independent experiments. (**d**) Groups of 3 C57Bl/6 mice bearing s.c. EG7-OVA tumors were i.v. injected with 15 × 10^{6} OT-1 effector T-cells bearing surface-conjugated with DiD-labeled NPs (100 NPs/cell, filled bars), an equivalent number of DiD-labeled particles alone (open bars). After

48 h indicated tissues were removed, weighed, and macerated with scissors. We quantified specific DiD tissue fluorescence for each organ using the IVIS Spectrum imaging system and calculated the mean percentage of injected dose per gram of tissue (%ID g^{-1}) as final readout (**d**). Data shown are pooled from three independent experiments.

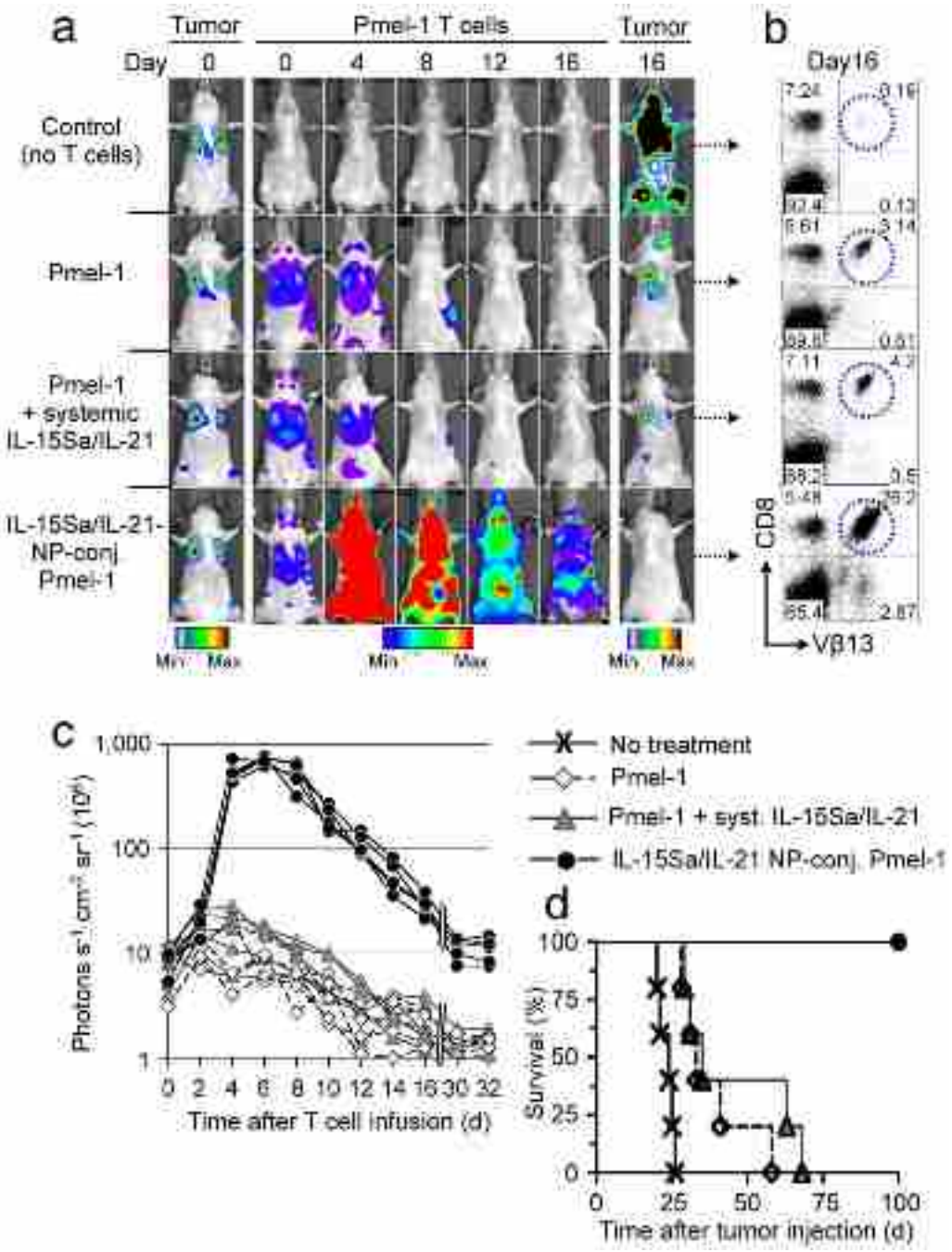

Figure 4.

Pmel-1 T-cells conjugated with IL-15Sa/IL-21-releasing NPs robustly proliferate *in vivo* and eradicate established B16 melanomas. Lung and bone marrow tumors were established by tail vein injection of 1×10^6 Gaussia luciferase-expressing B16F10 cells in C57Bl/6 mice. Tumor-bearing animals were treated after 1 week by sublethal irradiation followed by i.v. infusion of 10×10^6 Click beetle red luciferase-expressing $V\beta13^+CD8^+$ Pmel-1 T-cells. One group of mice received Pmel-1 T-cells conjugated with 100 NPs/cell carrying a total dose of 5 μg IL-15Sa/IL-21 (4.03 μg IL-15Sa + 0.93 μg IL-21), control groups received unmodified

Pmel-1 T-cells and a single systemic injection of the same doses of IL-15Sa/IL-21 or Pmel-1 T-cells alone. (**a**) Dual longitudinal *in vivo* bioluminescence imaging of Gaussia luc-expressing B16F10 tumors and CBR-luc-expressing Pmel-1 T-cells. (**b**) Frequencies of $V\beta13^{+}CD8^{+}$ Pmel-1 T-cells recovered from pooled lymph nodes of representative animals 16 days after T-cell transfer. (**c**) CBR-luc T-cell signal intensities from sequential bioluminescence imaging every two days after T-cell transfer. Every line represents one animal with each dot showing the whole animal photon count. (**d**) Survival of animals following T-cell therapy illustrated by Kaplan-Meier curves. Shown are six mice/treatment group pooled from three independent experiments.

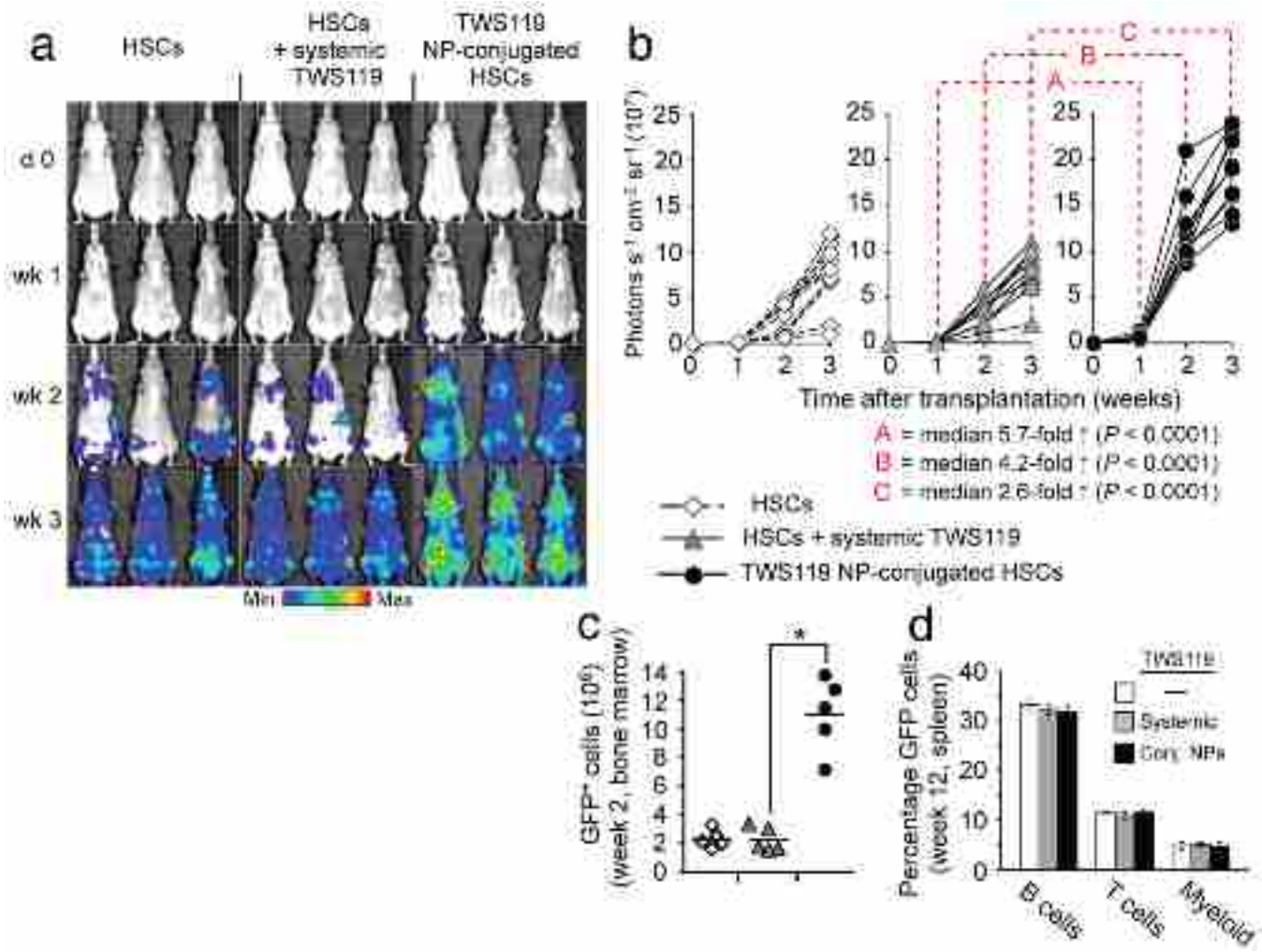

Figure 5.

HSCs carrying GSK-3β inhibitor-loaded nanoparticles reconstitute recipient animals with rapid kinetics following bone marrow transplants without affecting multilineage differentiation potential. (**a**,**b**) Engraftment kinetics of luciferase-transgenic HSC grafts in lethally-irradiated nontransgenic syngeneic recipients. Mice were treated with a single bolus injection of the GSK-3β inhibitor TWS119 (1.6 ng) on the day of transplantation, an equivalent TWS119 dose encapsulated in HSC-attached NPs, or no exogenous adjuvant compounds. Transplanted mice were imaged for whole-body bioluminescence every seven days for three weeks. Shown are representative IVIS images (**a**) and whole animal photon counts (**b**) for nine mice total/treatment condition. (**c**) Percentage of donor-derived cells two weeks after transplantation of GFP^+ HSCs into lethally-irradiated recipients with or without TWS119 adjuvant drug. $*P < 0.001$. (**d**) Average frequency of donor-derived GFP^+ B-cells, T-cells, and myeloid cells in recipient mice three months after transplantation. five mice/group were analyzed.